separations

MDPI

Article

Shaping of HKUST-1 via Extrusion for the Separation of CO_2/CH_4 in Biogas

Muhamad Tahriri Rozaini [1,2], Denys I. Grekov [2], Mohamad Azmi Bustam [1,*] and Pascaline Pré [2,*]

[1] Centre of Research in Ionic Liquids, CORIL, Chemical Engineering Department, Universiti Teknologi Petronas, Bandar Seri Iskandar 32610, Perak, Malaysia
[2] IMT Atlantique, GEPEA UMR-CNRS 6144, 44307 Nantes, France
* Correspondence: azmibustam@utp.edu.my (M.A.B.); pascaline.pre@imt-atlantique.fr (P.P.)

Abstract: HKUST-1 is a metal-organic framework (MOF) that is widely studied as an adsorbent for CO_2 capture because of its high adsorption capacity and good CO_2/CH_4 selectivity. However, the numerous synthesis routes for HKUST-1 often result in the obtention of MOF in powder form, which limits its application in industry. Here, we report the shaping of HKUST-1 powder via the extrusion method with the usage of bio-sourced polylactic acid (PLA) as a binder. The characterization of the composite was determined by XRD, FTIR, TGA and SEM analyses. The specific surface area was determined from the N_2 adsorption isotherm, whereas the gas adsorption capacities were investigated via measurements of CO_2 and CH_4 isotherms of up to 10 bar at ambient temperature. The material characterization reveals that the composite preserves HKUST-1's crystalline structure, morphology and textural properties. Furthermore, CO_2 and CH_4 adsorption isotherms show that there is no degradation of gravimetric gas adsorption capacity after shaping and the composite yields a similar isosteric adsorption heat as pristine HKUST-1 powder. However, some trade-offs could be observed, as the composite exhibits a lower bulk density than pristine HKUST-1 powder and PLA has no impact on pristine HKUST-1's moisture stability. Overall, this study demonstrates the possibility of shaping commercial HKUST-1 powder, using PLA as a binder, into a larger solid-state-form adsorbent that is suitable for the separation of CO_2 from CH_4 with a well-preserved pristine MOF gas-adsorption performance.

Keywords: shaping; HKUST-1; MOF-polymer composite; extrusion

Citation: Rozaini, M.T.; Grekov, D.I.; Bustam, M.A.; Pré, P. Shaping of HKUST-1 via Extrusion for the Separation of CO_2/CH_4 in Biogas. *Separations* **2023**, *10*, 487. https://doi.org/10.3390/separations10090487

Academic Editor: Dimosthenis Giokas

Received: 30 June 2023
Revised: 31 July 2023
Accepted: 16 August 2023
Published: 6 September 2023

1. Introduction

Biogas possesses significant potential as an alternative energy source, addressing the ever-increasing global energy demand while simultaneously mitigating waste and greenhouse gas (GHG) emissions. Various organic wastes, such as sewage sludge, agricultural and crop residues, animal dung, and industrial organic wastes and wastewaters, can be transformed into biogas via the process of anaerobic digestion. The major constituents of biogas are methane (CH_4; 40–75%) and carbon dioxide (CO_2; 15–60%), with traces of nitrogen (N_2; 0–5%), moisture (H_2O; 1–5%) hydrogen sulphide (H_2S; 0–5000 ppm), oxygen (O_2; 0–2%), ammonia (NH_3; 0–500 ppm) and other trace gases [1]. Furthermore, the potential of biogas usage is huge, with the predicted demand for biogas (either directly used or purified) by the International Energy Agency (IEA) reaching up to 150 Mtoe by 2040 [2].

Biogas can be directly burned to produce heat and energy; however, the presence of noncombustible CO_2 in biogas decreases its calorific value. Therefore, biogas could be purified by removing its contaminants to obtain biomethane. The process of removing biogas contaminants, especially CO_2, is known as biogas upgrading.

Biomethane (also known as renewable natural gas) is indistinguishable from natural gas and can be transported and used in the same way. Biomethane can deliver the energy system benefits of natural gas while being carbon-neutral. At present, multiple technologies exist in the industry for CO_2 separation and capture for biogas upgrading, such as

water/physical/chemical scrubbing, cryogenic separation, membrane separation, and the technology that interests us in this work: pressure swing adsorption [3–6]. The adsorption process for CO_2 capture presents its advantages as a dry process, which means it does not require the additional costs of water/solvent, nor does it have a heat requirement for the regeneration of the adsorbent, as is found in other CO_2 removal technologies. Furthermore, the adsorption unit is relatively small, compact, and easily manufactured for small-scale applications. The adsorbent choice in the adsorption column is one of the key factors influencing the CO_2 removal efficiency in the adsorption process. Each adsorbent has different properties that need to be considered for application, such as adsorption and pressure swing regeneration capacities, selectivity, and mechanical and thermal stability over long lifetimes. Adsorbents commonly used in the adsorption process include zeolite and carbon-based microporous solids [7].

One of the potential new adsorbents for CO_2 capture in biogas-upgrading applications is the metal-organic framework (MOF). MOFs are two- or three-dimensional, porous, crystalline materials, synthesized by joining metal-containing units with organic linkers [8,9]. Thanks to their high specific surface area, high porosity, and tunable properties [10,11], MOFs have become potential candidates as a novel adsorbent media for gas separation [12,13]. Studies have been conducted that demonstrate MOFs' CO_2 capture abilities in CO_2/CH_4 mixtures [14–17]. HKUST-1 is one of the most frequently studied MOFs in the literature for application in CO_2 capture due to its high CO_2-adsorption capacity and good CO_2/CH_4 selectivity [18,19]. HKUST-1 can also be synthesized via different synthesis routes, such as the conventional synthesis methods of solvothermal [20,21], microwave [22,23], sonochemical [24], electrochemical [25,26], and mechanochemical synthesis [27,28].

As obtained from such synthesis routes, the HKUST-1 adsorbent occurs as a fine crystalline powder that needs to be shaped into granules or monoliths to constitute the adsorbent beds, generating low-pressure drops and a uniform gas flow [29,30]. Driven by the need to enhance MOFs' applicability in industrial applications, studies on MOF shape engineering have been attracting attention in recent years [31–34].

Extrusion is one of the many reported shaping technologies for MOF powders. The mechanism of extrusion relies on passing the pre-formed paste (which normally constitutes a mixture of the MOF powder and a binding agent) inside an extruder through a die. Depending on the form of the die, the final objects can have different shapes: hollow tubes, sheets, strips, or cylinders. Ideally, the shaping of MOF powders should result in a material with strong mechanical and thermal properties, as well as a good adsorption performance. Nevertheless, the use of a binding agent in the extrusion-shaping technique presents a challenge in obtaining shaped MOFs with the previously mentioned desirable characteristics, as a binding agent could cover the surface of the crystallite and hence block the MOF's pores.

As an example, Hong et al. shaped MIL-101 (Cr) powder into monoliths using bentonite clay as the binding agent via the extrusion method [35]. The resulting shaped monolith suffered an approximately 10–34% reduction in specific surface area and a decrease in the CO_2 adsorption capacity by 36.81% in comparison to pristine MIL-101 (Cr). On the other hand, the usage of bentonite as a binding agent helped to promote the mechanical strength of the monolith, with a radial compression of 10.60 N/mm^2 and 4.97 N/mm^2 when the binding content was reduced from 40% (w/w) to 35% (w/w), respectively.

Additionally, studies on HKUST-1 extrusion were performed by Majano and Pérez-Ramírez by shaping HKUST-1 powder with 20 wt% kaolin as the binder [36]. An XRD analysis of the extrudate confirmed that the crystal structure was preserved upon extrusion but suffered a reduction of approximately 50% in its initial specific surface area. Both these studies indicate the difficulties in shaping MOF crystal powder into a larger solid-state material without altering its intrinsic adsorption properties. The addition of a binding agent often leads to improved mechanical stability but degrades the adsorption performance.

In this work, HKUST-1 powder was shaped via the extrusion method using bio-sourced polylactic acid (PLA) as the binding agent to produce the extrudate composite. The impact of shaping on composite adsorption performance was further elucidated by the investigation of its structural and textural properties compared to pristine HKUST-1. Furthermore, the adsorption equilibrium for CO_2 and CH_4 for both the extrudate composite and pristine HKUST-1 were determined to match the applicability criteria for gas separation in the pressure swing adsorption process.

2. Materials and Methods

2.1. Materials

HKUST-1, also commercially known as Basolite@C300 (Basolite is a trademark of BASF SE), was supplied by Sigma Aldrich (Darmstadt, Germany). According to the supplier, the specific surface area was in the range of 1500–2100 m^2/g and the bulk density was 0.35 g/cm^3. The degassing of samples was carried out at 473 K under vacuum.

2.2. Shaping of HKUST-1

Figure 1 illustrates the shaping process of HKUST-1 powder with PLA. In brief, the homogenous mixing of HKUST-1 with PLA was achieved by dissolving 0.1 g of PLA in 1 mL of solvent (chloroform) using a VWR Symphony ultrasonic bath at 328 K for 1 h. Prior to dissolving the PLA, it was heated at 383 K to eliminate any possible water traces. Next, 0.9 g of HKUST-1 was added to the solution and sonicated for another 30 min to ensure homogenous mixing. The HKUST-1/PLA suspension was then inserted into a 5 mL DB syringe before being extruded into a methanol solution that did not dissolve the PLA. This immersion promotes the phase inversion and the transfer of chloroform from the HKUST-1/PLA suspension to methanol, resulting in the formation of a solid HKUST-1/PLA composite. The composite was then heated at 38 K under vacuum overnight to remove the traces of methanol. The dried composite, with 10% weight in PLA, was then cut into small cylinders of about 1.5 mm, and is hereafter referred to as the extrudate.

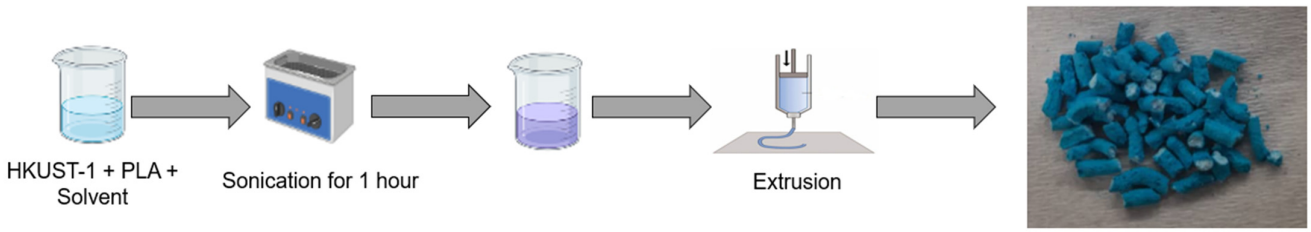

Figure 1. Schematic figure of the HKUST-1-shaping procedure in this work.

2.3. Sample Characterization and Gas Adsorption Measurement

The crystalline structure of the samples was confirmed using powder X-ray diffraction (XRD). XRD patterns were recorded using Panalytical X'Pert^3 Powder (Malvern Panalytica, Almelo, The Netherlands) with Cu Kα radiation (λ = 1.5406 Å at 45 kV and 40 mA) at room temperature. Diffraction data were collected at a scan rate of 1°/min, step size of 0.02° and a 2θ range of 5–40. A Fourier Transform Infrared Spectroscopy (FTIR) spectrum was analyzed by the KBr technique using Thermo Nicolet IS5 (Waltham, MA, USA) with a wavenumber ranging from 5000 to 400 cm^{-1}, with 15 scans.

The morphology of the samples was observed using scanning electron microscopy (SEM) images acquired on EVOLS15 from ZEISS (Jena, Germany) equipped with a secondary electron detector (SE). The samples were prepared using a standard metallographic specimen preparation technique, where the cast sample was deposited onto a conductive carbon double-sided adhesive tape on a stub. Coating of the sample was effectuated with a platinum sputter coater for 60 s. The sample was placed in a vacuum chamber before the imaging was carried out.

Thermogravimetric analysis (TGA) measurements were performed on a STA 6000 instrument from Perkin Elmer (Waltham, MA, USA) in order to assess material thermal stability. A temperature ramp was applied from 313 K to 1073 K at 10 °C/min under a flow of nitrogen gas to avoid sample oxidation. The blank was subtracted to correct the TG signal.

N_2 adsorption/desorption isotherm analysis at 77 K was conducted to characterize the textural properties of the materials using a 3Flex manometric adsorption analyzer (Micromeritics, Norcross, GA, USA). The equipment is capable of measuring the experimental data in the range of relative pressure (P/P_o) between 10^{-7} and 1, with a precision of 0.15%. The acquisition of experimental data was first performed in a "fixed-dose" mode until $P/P_o = 0.03$, followed by the "incrementing relative pressure" mode until $P/P_o = 1$. Additionally, the equilibration time period was set to 90 s for the analysis in the domain of micropore-filling. Prior to analysis, the sample was degassed at 398 K under vacuum for at least 72 h using Smart VacPrep (Micromeritics, Norcross, GA, USA). The volumes of the cell non-occupied by sample were determined at ambient temperature and at 77 K by helium expansion. Apparent specific surface area was determined based on the linearized BET isotherm derived from the assumptions made by the BET theory:

$$\frac{P/P_o}{N\,(1-P/P_o)} = \frac{1}{N_m C} + \frac{C-1}{N_m}\left(\frac{P}{P_o}\right) \quad (1)$$

where N is defined as the adsorbate loading, P_o is the saturation pressure of nitrogen, C corresponds to the energetics of adsorption and N_m relates to the monolayer loading. C and N_m are constant values which allow for the determination of the specific surface area of the materials (otherwise known as BET surface area). The selected pressure range was chosen in the domain of $10^{-7} \leq P/P_o \leq 10^{-2}$ to respect the four consistency criteria suggested by Rouquerol et al. [37], which are:

1. Only a pressure range where $N\,(1 - P/P_o)$ increases monotonically with P/P_o should be selected.
2. The value of the C constant obtained from the linear regression must be positive.
3. The value of relative pressure P/P_o, which corresponds to the monolayer loading N_m, must be within the selected pressure range chosen in criterion 1.
4. The value of $(1/\sqrt{C} + 1)$ should be equal to the relative pressure determined in criterion 3. (Tolerance up to 20% is suggested by Rouquerol et al. [37].)

Bulk density is defined as the mass divided by the total volume filled by the material, which includes solid and internal particle pore volumes, as well as inter-particle void volume. The bulk density of the extrudate was determined after extrudate samples settled to a stable formation inside a recipient with known volume following light tapping.

The mechanical resistance of the shaped MOF composite against the frictional forces experienced in fluidized or packed beds, transportation, handling, and storage was evaluated through the attrition test standard D4058-96 ASTM norm. In this work, a standard test similar to that employed by Khabzina et al. [38] was applied. In brief, 0.2 g mass of material was introduced into a glass vial and rolled at a frequency of 60 rotations per minute (rpm) for 30 min. Afterwards, the sample was passed through a 500 µm sieve to recover fine particles. Attrition percentage was calculated as follows:

$$\text{Attrition} = \frac{\text{initial mass} - \text{recovered mass above 500 µm}}{\text{initial mass}} \times 100 \quad (2)$$

CO_2 and CH_4 adsorption isotherm measurements were conducted at 273 K, 298 K and 323 K using PCT-Pro manometric equipment from SETARAM (Caluire, France) for a range of pressure up to 10 bar, and 3Flex from Micromeritics (up to 1 bar). Prior to each measurement, the samples were degassed under dynamic vacuum at 393 K for 12 h, and the sample holder's dead volume was measured using helium expansion.

2.4. Isosteric Heat of Adsorption

The isosteric heat of adsorption provides a quantitative assessment of the strength of interactions between the adsorbate and the adsorbent, offering valuable information regarding the energetic heterogeneity exhibited by a solid surface. The measured adsorption isotherms of CO_2 were used to calculate the isosteric heats of adsorption using the Van't Hoff equation:

$$\ln \frac{P_2}{P_1} = \frac{Q_{is}}{R} \times \left(\frac{1}{T_1} - \frac{1}{T_2}\right) \quad (3)$$

where Q_{is} is the isosteric heat of adsorption and R is the universal gas constant with a value of 8.314 J/mol K. Data from isotherms at three different temperatures were used to plot the logarithm of the equilibrium pressures ln(P) against the reciprocal temperature (1/T) at the constant CO_2 uptake to estimate the value of Q_{is}.

2.5. Prediction of CO_2/CH_4 Co-Adsorption Isotherm and Selectivity via Ideal Adsorbed Solution Theory (IAST)

Ideal adsorption solution theory was developed by Myers and Prausnitz [39] to provide a solid theoretical foundation to predict multi-component adsorption isotherm from single, pure component adsorption isotherm data. IAST relies on the assumption that the adsorbed species form an ideal mixture at a constant spreading pressure and temperature so that the activity coefficient of each phase reaches unity.

The selectivity was calculated with the aid of IAST++ program to assess the separation performance of HKUST-1 powder and HKUST-1/PLA extrudate for the CO_2/CH_4 mixture at 298 K [40]. The calculation of IAST selectivity using this software can be summarized in two steps: (1) fitting suitable isotherm models to the adsorption isotherm data of pure gases, and (2) resolution of mixed gas adsorption isotherm using fitted model parameters. In our study, the fitting of CO_2 and CH_4 adsorption isotherms was carried out using the dual-site Langmuir model, which can be expressed as:

$$q_i = q_{1,i} \cdot \frac{k_{1,i}P}{1 + k_{1,i}P} + q_{2,i} \cdot \frac{k_{2,i}P}{1 + k_{2,i}P} \quad (4)$$

where $q_{1,i}$ and $q_{2,i}$ are the saturation capacity of component i in the gas mixture at site 1 and site 2, respectively; $k_{1,i}$ and $k_{2,i}$ are the equilibrium constant of component i in the gas mixture at site 1 and site 2; P is the pressure of the bulk gas at equilibrium with the adsorbed phase; and q_i is the amount of component i that is absorbed.

The IAST-equilibrium selectivity $\alpha_{i/j}$ was derived from the distribution of the molar fractions of the components in both the gas and adsorbed phases measured under equilibrium conditions:

$$\alpha_{i/j} = \frac{x_i / y_i}{x_j / y_j} \quad (5)$$

where x_i and x_j are the molar fraction of components i and j in the adsorbed phase, and y_i and y_j are the molar fractions of components i and j in the gas phase.

2.6. Humidity Ageing Analysis

Ageing of the materials was performed by storing HKUST-1 powder and extrudate inside a room with a controlled temperature of 298 ± 5 K and relative humidity (RH) of 40 ± 5% for a duration of 1 month. The stored samples were then re-characterized via N_2 adsorption/desorption isotherm at 77 K and their adsorption capacity was re-measured by conducting CO_2 adsorption isotherms of up to 1 bar at 298 K.

3. Results and Discussion

3.1. XRD Analysis

A structural analysis of the HKUST-1/PLA composite was carried out through XRD analysis. Figure 2 illustrates the XRD peaks for HKUST-1/PLA extrudate, PLA and pristine

HKUST-1 powder. Neat PLA exhibits a strong peak at 2θ = 16.8° because of diffraction from (110) and/or (200) planes [41]. Interestingly, diffraction peaks corresponding to the neat PLA cannot be clearly distinguished in the XRD peaks of the extrudate, likely due to the low loading amount of PLA present in the composite.

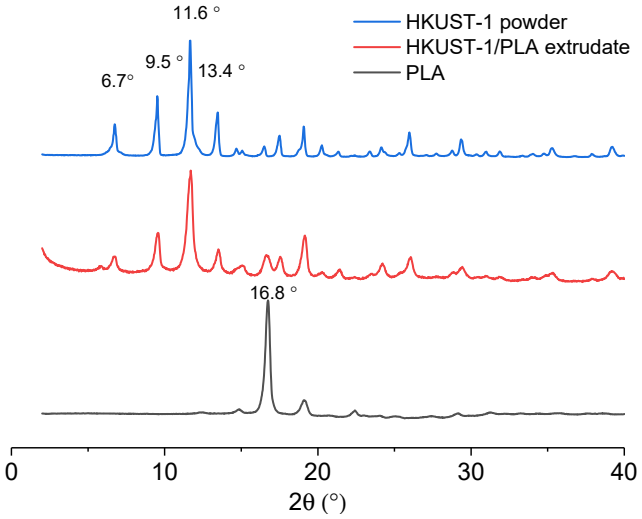

Figure 2. XRD of HKUST-1 powder, neat PLA and HKUST-1/PLA extrudate.

HKUST-1 powder exhibits XRD peaks at 6.7°, 9.5°, 11.6° and 13.4°, which can be assigned to the (200), (220), (222) and (400) crystal planes of HKUST-1 [42,43]. The extrudate clearly exhibits similar peaks associated with HKUST-1 powder, which shows that the shaping of HKUST-1 via extrusion has conserved crystal particle morphology.

3.2. FTIR Analysis

Analysis of FTIR spectra enables further analysis of the composition of the shaped composites. Figure 3 shows the FTIR spectra of HKUST-1/PLA extrudate, pristine HKUST-1 and PLA. PLA is made up of lactic acid, which is rich in carbon-chain-containing C=O groups. The band of this carbonyl group could be assigned to the peak observed at 1750 cm^{-1} for both the PLA and the extrudate sample. In addition, HKUST-1/PLA extrudate exhibits peaks at 1184 cm^{-1} and 1090 cm^{-1}, which could be assigned to the symmetric and antisymmetric stretching vibration of the C-O groups [44].

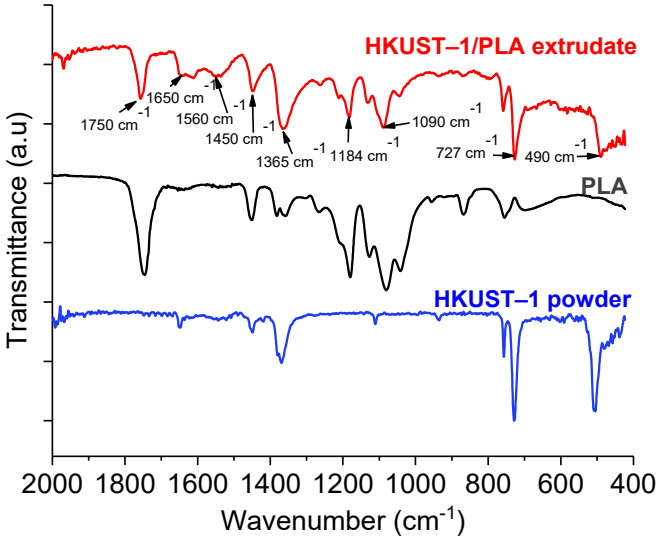

Figure 3. FTIR of HKUST-1 powder, neat PLA and HKUST-1/PLA extrudate.

HKUST-1/PLA extrudate also exhibits similar bands to the pristine HKUST-1 powder. Both HKUST-1 powder and HKUST-1/PLA extrudate exhibit characteristic asymmetric vibrations of carboxylate groups at 1500–1700 cm^{-1} ranges and symmetric vibrations at 1300–1500 cm^{-1} ranges [45]. The peak at 1650 cm^{-1} is assigned to the C=O stretching vibration of deprotonated benzene tricarboxylic acid [46], whereas the bands at 490 cm^{-1} and 727 cm^{-1} correspond to the copper-oxygen bond (Cu-O) and aromatic C-H bending of benzene rings [47,48]. The presence of typical bands of neat PLA and HKUST-1 powder in the extrudate show the presence of both materials in the composite, verifying that the shaping of HKUST-1 with PLA via extrusion was successful.

3.3. SEM Analysis

The characterization of HKUST-1/PLA surface morphology was achieved through Scanning Electron Microscopy (SEM) analysis. Figure 4 shows a morphology comparison of pristine HKUST-1 powder and HKUST-1/PLA extrudate. It could be observed that the particles of HKUST-1 pristine powder exhibit an octahedron shape, which is the reported morphology of Basolite C300 [49]. The surface analysis of HKUST-1/PLA extrudate shows that HKUST-1 particles kept their octahedron shape, and their surface remained accessible.

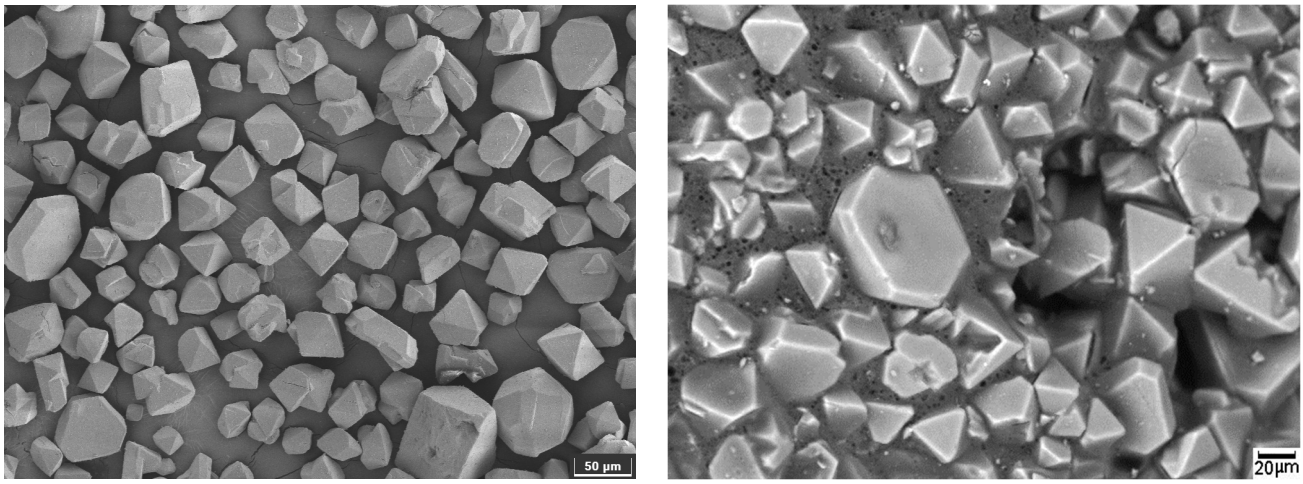

(**a**) (**b**)

Figure 4. (**a**) SEM image of HKUST-1 powder; (**b**) SEM image of HKUST-1/PLA extrudate.

This finding suggests that the shaping of HKUST-1 powder via extrusion maintains the morphology of HKUST-1 particles in the composite, with no obvious cleaving/destruction of the particles, as the shaping process did not involve high pressurization. Most of the HKUST-1 particles in the extrudate sample were exposed and not encapsulated by the PLA due to the low loading amount of the PLA binder.

3.4. Thermal Stability Analysis

The TGA profiles for HKUST-1 powder, neat PLA and HKUST-1/PLA extrudate are shown in Figure 5. Both pristine HKUST-1 and PLA are thermally stable up to 593 K and 613 K, respectively, above which mass losses become observable. In contrast, the thermal stability of HKUST-1/PLA extrudate appears to be far lower than that of pristine HKUST-1 powder and neat PLA, as mass losses are detected at 323 K. Meanwhile, thermal degradation of the extrudate proceeds in two steps. It is possible that the initial mass loss between 323 and 393 K is caused by trapped chloroform solvent molecules departing. The degradation of PLA and the subsequent framework collapse can be linked to the second mass loss, which begins at 578 K.

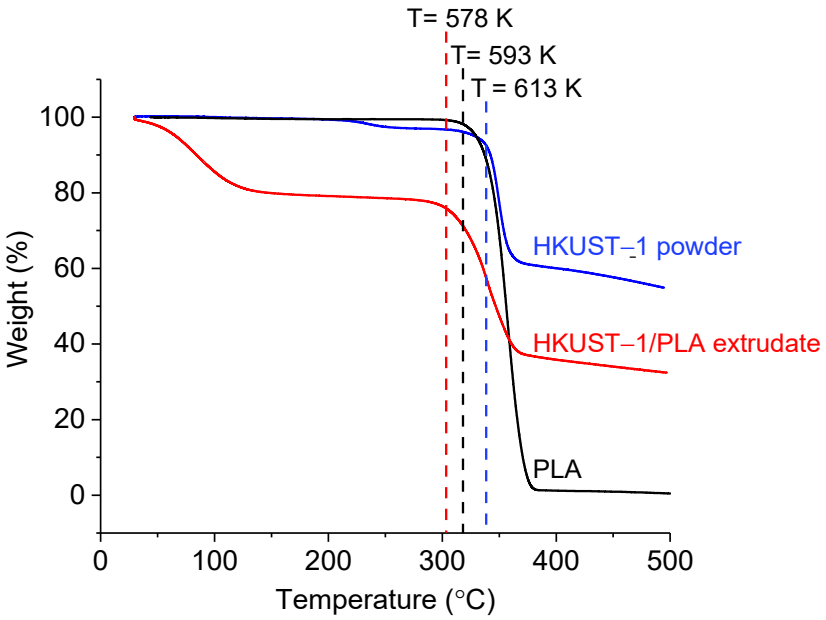

Figure 5. TGA profile for HKUST-1 powder, PLA and HKUST-1/PLA extrudate.

The results suggest that the presence HKUST-1 in the composite decreases its thermal stability, as HKUST-1 particles may act as catalysts for the pyrolysis of PLA. A similar observation of decreasing thermal stability in PLA in the presence of MOF particles has been observed in several studies [41,50].

3.5. Physical Properties and Mechanical Stability Analysis

The specific surface areas of samples were determined using the BET model applied to nitrogen adsorption isotherms measured at 77 K. The isotherm linear and logarithmic plot between HKUST-1 powder and HKUST-1/PLA extrudate is shown in Figure 6. It can be seen that similar patterns of N_2 uptake were measured for both the pristine HKUST-1 powder and the extrudate. These are characteristic of type I isotherms, relevant to highly microporous materials. The large N_2 adsorption capacity exhibited by the extrudate could be linked back to the SEM particle morphology observations: the HKUST-1 crystal particles are not encapsulated by the PLA matrix; hence, their porosity remains accessible to N_2 adsorption. PLA itself is a non-porous polymer and exhibits a very low BET surface area (Supplementary Figure S1 and Table S1), which signifies that higher loading amounts of PLA in the composite may increase the risk of HKUST-1 particle encapsulation, hindering their accessibility to gas.

The adsorption of N_2 in the low-pressure region ($P/P_o < 10^{-4}$) is noticeably higher for the extrudate than the pristine HKUST-1, which suggests that there are changes in material microporosity after shaping. Table 1 lists the BET surface area and pore volume data for both pristine HKUST-1 powder and the extrudate. A BET surface area of 1528 m^2/g was obtained for the extrudate, which is comparable to the HKUST-1 pristine (1500 m^2/g). It can be observed that the measured micropore volume is slightly higher than that of the pristine HKSUT-1 powder, which confirms the changes in microporosity, as previously mentioned. We assumed that these changes may result from the effect of washing, by immersion of the HKUST-1 composite in the methanol solution at the final step in the shaping process, as methanol is very effective in removing impurities inside the pores of HKUST-1 [51,52].

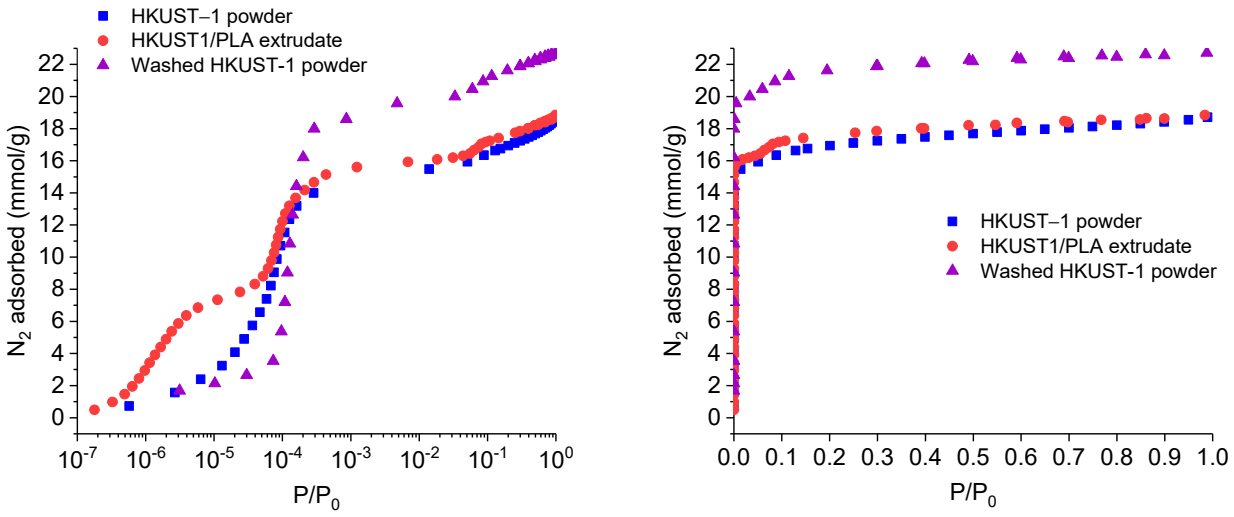

Figure 6. Logarithmic (**a**) and linear (**b**) N_2 adsorption isotherm plot for HKUST-1 powder, HKUST-1/PLA extrudate and washed HKUST-1 powder.

Table 1. BET surface area, pore volume of pristine HKUST-1 powder, and HKUST-1/PLA extrudate.

Sample	S_{BET} (m^2/g)	Micropore Volume (cm^3/g), [a]	Total Pore Volume (cm^3/g), [b]
HKUST-1 powder	1500	0.46	0.65
HKUST-1/PLA extrudate	1528	0.54	0.65
Washed HKUST-1 powder	1956	0.60	0.79

[a] Micropore volume determined by applying t-plot method to N_2 adsorption data. [b] Total pore volumes were calculated from experimental N_2 sorption data at P/P_o = 0.98.

To verify that immersion in methanol influences the porosity and BET surface area of HKUST-1, pristine MOF powder was washed in methanol for three times (hereafter, this will be referred to as "washed HKUST-1 powder") and subsequently re-characterized via N_2 adsorption isotherm at 77 K, as reported in Figure 6. It can be observed that after washing with methanol, the amount of adsorbed N_2 by HKUST-1 increases significantly in the upper relative pressure range above 10^{-4}, but remains low below this range. The washed HKUST-1 powder yielded a BET surface area and pore volume higher than both the pristine HKUST-1 powder and the extrudate, but these do not completely explain the discrepancies observed in the lowest relative pressure region for the extrudate sample. Hence, the reason for the changes in the microporosity of the extrudate is still unknown. For the subsequent section, we retained the comparison of the extrudate properties with pristine HKUST-1 powder only, as the shaping of the extrudate involved the direct usage of HKUST-1 powder as-is, without pre-washing with methanol.

The bulk density of the extrudate was measured at 0.25 g/cm^3, which is lower than the bulk density of the pristine HKUST-1 (0.35 g/cm^3). This lower density can be attributed to the shaping extrusion technique, which is applied at a low mechanical pressure, resulting in dissimilar crystallite packing and, therefore, a large fraction of void space in the extrudate sample.

MOFs shaped with PLA need to have good mechanical resistance to attrition for use as adsorbent materials in gas separation processes. Because of particle attrition, bed clogging or increases in pressure drops may occur. Table 2 compares the attrition test data measured for the HKUST-1/PLA with those of commercially available molecular sieve adsorbents and MOF extrudate evaluated by the same test standard D4058-96 ASTM norm. The attrition loss of the extrudate sample was below 0.5 wt%, which is comparable with the attrition loss of the commercial shaped adsorbent and lower than the UiO-66 extrudate

reported in [38]. This shows that the mere addition of 10% loading in the mass of PLA as a binding agent suffices to create a mechanically robust adsorbent, while increasing the binder content would further enhance the attrition resistance. However, there is a risk of trade-offs between the increasing mechanical stability of the composite with adsorption capacity by increasing the PLA loading amount, as PLA is non-porous and may encapsulate HKUST-1 particles.

Table 2. Attrition percentage of HKUST-1/PLA extrudate, conventional adsorbent and MOF extrudate.

Sample	Attrition Loss (% wt)	Reference
HKUST-1/PLA extrudate	≤0.5	This work
3A	≤0.2	[53]
4A	≤0.2	
5A	≤0.2	
13X	≤0.2	
AC-Norit RZN_1	0.2	[38]
UiO-66 extrudate	1.4	

3.6. CO_2/CH_4 Adsorption

Figure 7 presents CO_2/CH_4 gravimetric and volumetric adsorption isotherms measured on pristine HKUST-1 powder and extrudate sample. The data were collected in the pressure range of up to 10 bar at 298 K. The gravimetric values were expressed in molar quantity adsorbed by 1 g of adsorbent/composite samples (mmol/$g_{adsorbent}$), whereas the volumetric adsorption capacity was expressed in molar quantity adsorbed by 1 cm^3 of volume occupied by adsorbent/composite sample (mmol/$cm^3{}_{adsorbent}$) by multiplying gravimetric adsorption capacities with the bulk density of the respective sample.

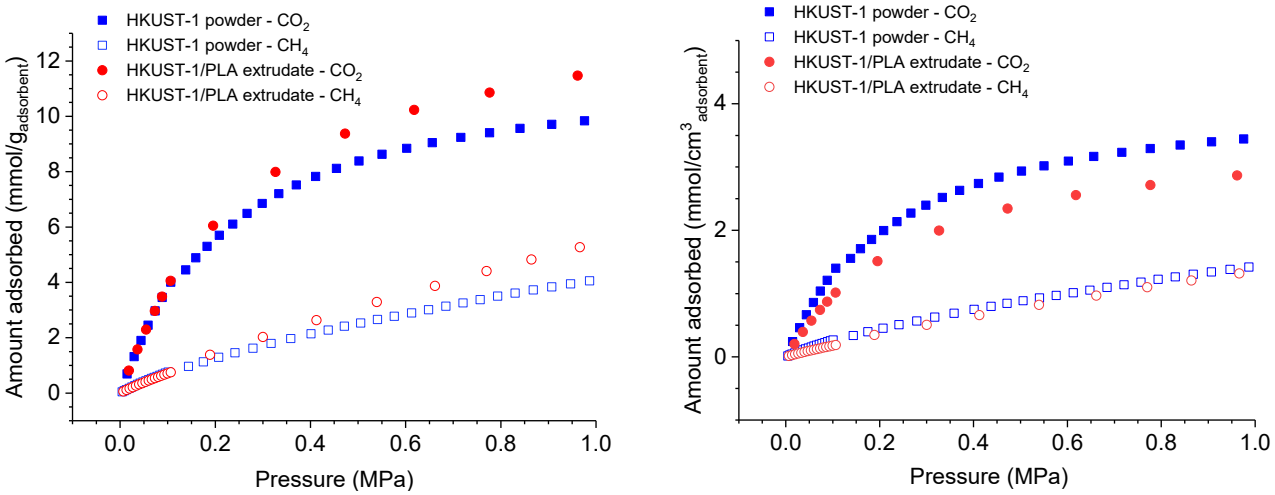

Figure 7. Gravimetric (**a**) and volumetric (**b**) adsorption isotherms of CO_2 and CH_4 on HKUST-1 powder and HKUST-1/PLA extrudate at 298 K.

The gravimetric adsorption capacity of both pristine HKUST-1 and extrudate are similar in the lower-pressure region of up to 1 bar. At higher pressures, between 2 and 10 bar, the CO_2 and CH_4 gravimetric adsorption capacities of the extrudate are slightly larger than those of pristine HKUST-1. Since PLA itself is nonporous and does not adsorb CO_2 or CH_4 (Figure S2), this increase could be attributed to the larger BET surface area and micropore volume of the extrudate, as observed earlier, and the enhancement of multimolecular adsorption thanks to the removal of impurities by methanol washing. However, because of its lower bulk density, the extrudate exhibits volumetric CO_2 adsorption capacities that are lower than those of pristine HKUST-1 in pressure ranges higher than 1 bar.

It is interesting to compare these data with those obtained for HKUST-1 powder that was activated with methanol prior to adsorption (washed HKUST-1 powder). Figure S3 shows the CO_2 gravimetric adsorption isotherm measured for the three samples in the low-pressure region. It could be observed that, at 1 bar, the CO_2 adsorption capacity of the washed HKUST-1 is 20% larger than the value measured for both pristine HKUST-1 powder and the extrudate. This can be attributed to the larger micropore volume of the washed HKUST-1 powder, whereas the lower adsorption capacity of the extrudate could be due to the substitution of 10 wt.% of porous material with a non-porous PLA binder and possibly partial pore blockage.

Table 3 provides a comparison with the literature data referring to gravimetric CO_2 adsorption capacities measured at 1 bar and 298 K on different MOF-polymer adsorbent composites shaped via extrusion. The data show that, compared to clay or other polymers, PLA appears to be a good candidate for use as a binding agent for MOF adsorbent shaping. Only one study [54] reported a similar conservation of the gravimetric CO_2 adsorption capacity at 1 bar after shaping MIL-53 (Al) with methyl cellulose binder at low loading rates. In [55], the HKSUT-1 extrudate synthesized with PVB as a binder exhibits an adsorption capacity reduced by 6% in comparison with that measured for pristine MOF powder. In [56], a shaped UTSA-16 extruded with PVA shows a CO_2 adsorption capacity that is lowered by 9% compared to pristine MOF. In [35], the high loading content of bentonite clay used as a binding agent resulted in a significant reduction in the CO_2 adsorption capacity of the Mil-1010 (Cr), by 47%.

Table 3. CO_2-adsorption capacities of MOF extrudate at 1 bar and 298 K.

Adsorbent	Binding Agent	Binding Agent Loading (wt.%)	Shaped MOF Adsorption Capacity (mmol/g)	Parent MOF Adsorption Capacity (mmol/g)	Reference
HKUST-1	Polylactic acid (PLA)	10	4.06	4.01	This work
MIL-53 (Al)	Methyl cellulose	3	2.60	2.60	[54]
HKUST-1	Polyvinyl butyral (PVB)	10	4.88	5.18	[55]
UTSA-16	Polyvinyl alcohol (PVA)	0.7	3.83	4.20	[56]
Mil-101 (Cr)	Bentonite clay	40	0.59	1.06	[35]

3.7. Isosteric Heat of Adsorption

The level of binding strength in the adsorbate-adsorbent interaction of an MOF material can be interpreted by the isosteric enthalpy of adsorption (Q_{is}). Figure 8 presents the CO_2/CH_4 isosteric heat of adsorption calculated from the Van't Hoff equation for extrudate, HKSUST-1 powder and benchmark zeolite 13X, which is frequently used as an adsorbent in the pressure swing adsorption process for biogas upgrading. The pure gas isotherm data needed for the calculation of benchmark 13X isosteric heat of adsorption were taken from [57], whereas isotherm measurements of the extrudate at different temperatures are presented in Figure S4.

The isosteric heat of adsorption for CH_4 at different adsorbate loadings was observed to be within a similar range (10–15 kJ/mol) for both HKUST-1 powder and extrudate. These values were lower than the respective CO_2 isosteric heat of adsorption, showing a lower affinity of CH_4 towards both samples. The CH_4 isosteric heat of adsorption for 13X was also found to be comparable to that of the HKUST-1/PLA extrudate sample. When comparing the CO_2 isosteric heat of adsorption among the HKUST-1 powder, extrudate, and 13X, it was observed that the latter exhibited a higher isosteric adsorption value (55–65 kJ/mol) compared to both HKUST-1 powder and the extrudate (20–25 kJ/mol). It can be concluded that HKUST-1/PLA extrudate retains its isosteric heat of adsorption

after shaping, offering an advantage in terms of requiring less energy for regeneration in a pressure swing adsorption process compared to 13X.

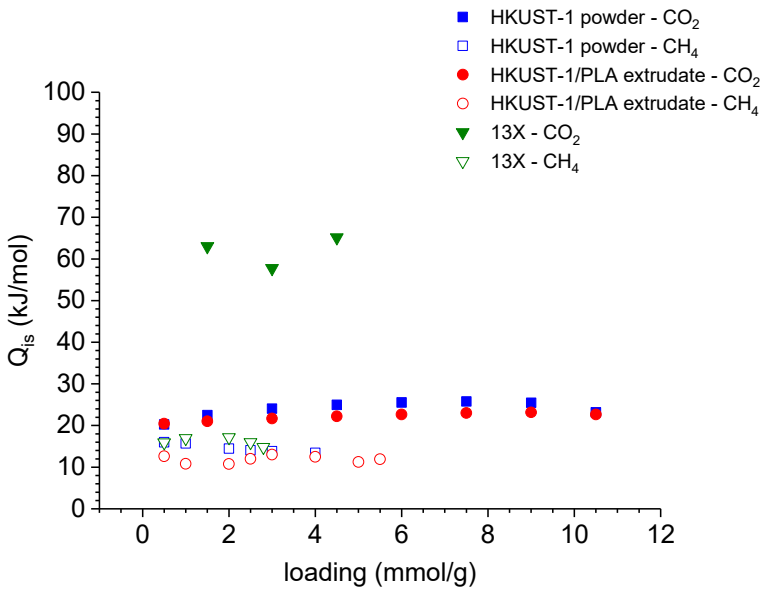

Figure 8. CO_2/CH_4 isosteric heat of adsorption for HKUST-1 powder, HKUST-1/PLA extrudate and 13X.

3.8. CO_2/CH_4 Co-Adsorption Isotherm and Selectivity Prediction in Gas Mixture

IAST relies on the assumption that the adsorbed species form an ideal mixture at a constant spreading pressure and temperature, in which the activity coefficient of each phase equals unity. IAST has been widely used to obtain various mixture isotherms for numerous systems validated by experimental measurements [58–61]. Table 4 lists the fitting parameters of the Langmuir isotherm model for the pure isotherms of CO_2 and CH_4 on HKUST-1 powder and HKUST-1/PLA extrudate. These fitting parameters were then used for the prediction of the adsorption isotherm of our samples in gas mixture.

Table 4. Fitting parameters of the dual-site Langmuir isotherm model for the pure isotherms of CO_2 and CH_4 on HKUST-1 powder and HKUST-1/PLA extrudate.

	HKUST-1 Powder		**HKUST-1/PLA Extrudate**	
	CO_2	**CH_4**	**CO_2**	**CH_4**
$q_{1,i}$ (mmol/g)	7.6819	0.693639	11.8369	3.97862
$q_{2,i}$ (mmol/g)	4.57812	16.0057	3.49004	117.582
$K_{1,i}$ (MPa^{-1})	4.24177	7.8488	3.2608	1.07153
$K_{2,i}$ (MPa^{-1})	4.24177	0.2778	3.2608	0.02949
R^2	0.9999	0.9999	0.9999	0.9999

Figure 9 presents the gravimetric co-adsorption isotherms HKUST-1 powder, extrudate and 13X (isotherm data obtained from [57]), predicted by IAST for a CO_2/CH_4 equimolar mixture, which represents biogas composition [1]. It could be observed that CO_2 is more preferably adsorbed on all samples compared to CH_4 in the mixed gas. The CO_2 and CH_4 gravimetric capacities of the extrudate were comparable to that of HKUST-1 pristine powder in the low-pressure range, but slightly larger in the upper pressure range. This suggests that the shaping method applied in our study did not degrade the adsorption selectivity of HKUST-1 in an equimolar CO_2-CH_4 gas mixture.

A comparison of predicted adsorption capacity for HKUST-1 extrudate with 13X in gas mixture is also interesting as it highlights the advantage of the HKUST-1/PLA extrudate in the pressure swing adsorption process. The working capacity of the adsorbent, which

is defined by the difference between the adsorbed quantities at production and purge pressures, is an important characteristic when choosing an adsorbent in PSA. Production pressure for biogas upgrading is around 8 bar [3], and the purge pressure is assumed to be 1 bar. With this operating condition, we can observe that the CO_2 working capacity of HKUST-1/PLA extrudate (6 mmol/g) is significantly higher than 13X (1.8 mmol/g), which shows the applicability of the extrudate in biogas upgrading.

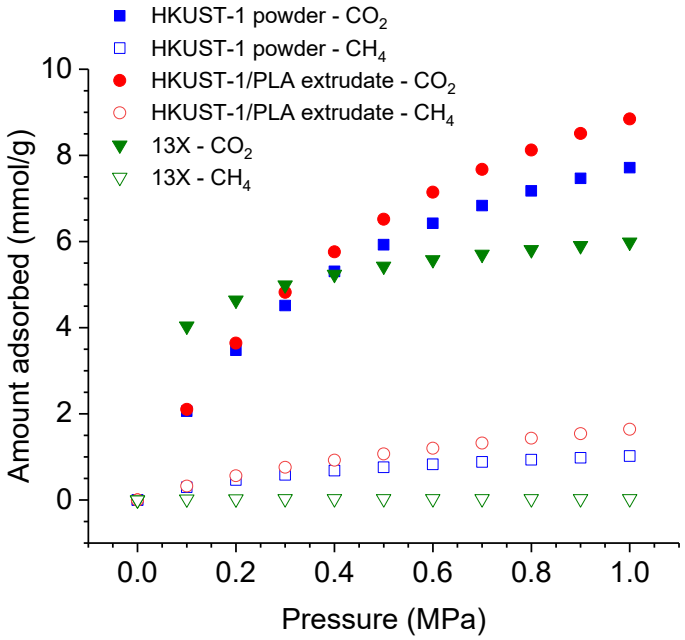

Figure 9. IAST-predicted isotherms for equimolar CO_2/CH_4 mixtures on HKUST-1 powder, HKUST-1/PLA extrudate and 13X at 298 K as a function of total bulk pressure.

The nature of CO_2 binding in 13X is related to the large quadruple moment (-13.71×10^{40}) of CO_2, which produces a strong attraction to the electrostatic field of the cationic site on the surface of 13X [62,63]. Meanwhile, the CO_2 binding on HKUST-1 is much weaker, as it is mainly of the van der Waals physisorption type [64,65]. This can be reflected in the value of isosteric heat of adsorption for CO_2 for 13X, which is higher than the extrudate, as highlighted in Section 3.7. Therefore, in the pressure region of 1–8 bar (operating pressure of biogas upgrading), the desorption of CO_2 from the extrudate is easier than 13X, explaining why the CO_2 working capacity of the former is higher.

Figure 10 presents the variations in the IAST-predicted selectivities of both pristine HKUST-1 and extrudate samples corresponding to the adsorption until equilibrium is reached for equimolar CO_2 and CH_4 mixtures over the pressure range of up to 10 bar, at 298 K. Interestingly, the CO_2/CH_4 selectivities of the extrudate slightly diminish as the bulk pressure increases, whereas the selectivity of pristine HKUST-1 powder does not vary as much with increasing bulk pressure. This difference in the selectivity changes may be related to the larger competitive CH_4-adsorption capacity of the extrudate, which lowers the separation selectivity. However, when comparing the selectivity value of extrudate with 13X, it can be observed that the value of the latter is significantly higher than that of the former because of the stronger affinity of CO_2 towards 13X compared to CH_4.

3.9. Ageing Analysis

It is a well-known fact that one of the disadvantages of HKUST-1 is that it is not stable in the presence of moisture, which results in a decrease in CO_2 adsorption capacity [66,67]. HKUST-1 can be considered a hydrophilic MOF, as Cu^{2+} ion of HKUST-1 has a very high affinity with water [68]. These copper ions are considered open-metal sites, as they are situated on the wall of the pores of MOF instead of being enclosed by a ligand. Therefore,

water molecules are adsorbed on these open metals, and the oxygen of the adsorbed H_2O shares a free electron pair with the Cu^{2+} ion, forming Cu-O bonds [69]. The prolonged exposure of HKUST-1 open-metal sites to water and the formation of Cu-O bonds will inevitably lead to the disintegration of the HKUST-1 framework [70]. Therefore, it is interesting to know whether PLA impacts the moisture stability of HKUST-1. Figure 11 presents the variations in BET surface area and CO_2 adsorption capacity at 1 bar, for HKUST-1 powder and the extrudate after 1 month of storage in relative humidity (RH) of 40 ± 5%. It can be observed that the degradation of BET surface area and CO_2 adsorption capacity are similar for both HKUST-1 powder and extrudate samples after 1 month, showing that PLA has no impact on the moisture stability of HKUST-1. Although the disadvantage of HKUST-1's moisture stability persists after shaping, this does not present a major problem in the application of biogas upgrading as, prior to the CO_2/CH_4 separation step in biogas upgrading, a pre-treatment process involving the removal of water/humidity is usually conducted [71,72].

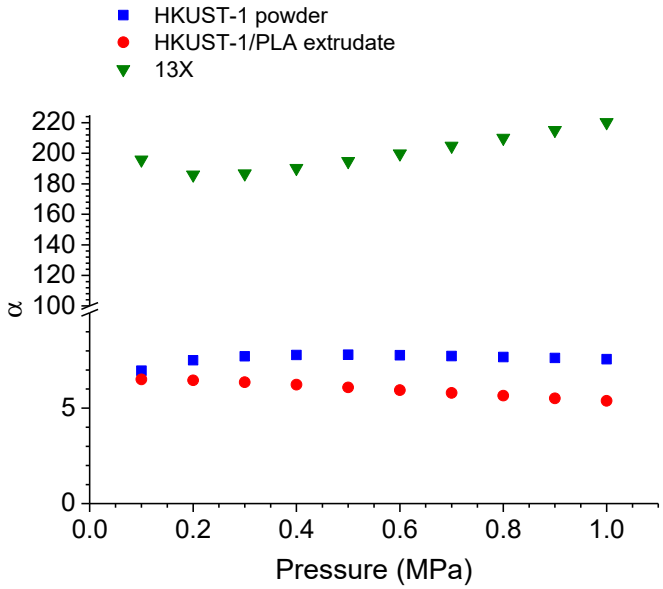

Figure 10. IAST-predicted selectivities to CO_2 and CH_4 for equimolar CO_2/CH_4 mixtures on HKUST-1 powder and HKUST-1/PLA extrudate at 298 K as a function of total bulk pressure.

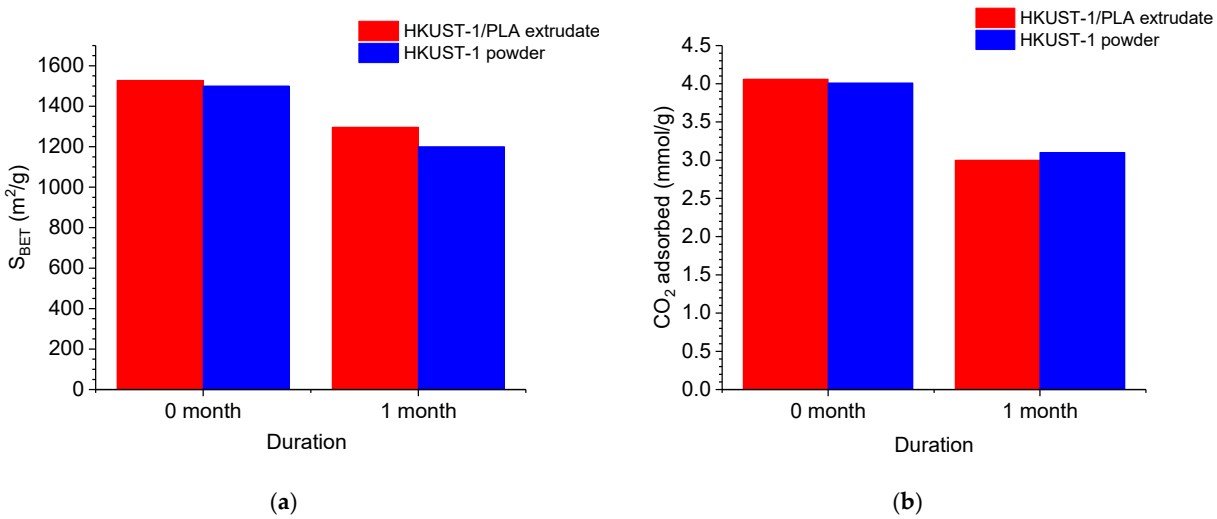

Figure 11. Variations in BET surface area (**a**) and CO_2 adsorption capacity (**b**) of HKUST-1 powder and HKUST-1/PLA extrudate stored in humid conditions for 1 month.

4. Conclusions

In this work, HKSUT-1 powders were shaped via an extrusion process, using PLA as a binding agent. XRD and FTIR analyses of the extrudate reveal well-preserved HKUST-1 particles within the composite, suggesting the successful shaping of HKUST-1 via extrusion. An SEM analysis of the extrudate reveals that the morphology of HKUST-1 particles was maintained, whilst a large fraction of their external surface appears accessible to gas. The extrudate also appears to decompose at a slightly lower temperature than the parent HKUST-1, which was attributed to the thermal degradation of PLA, which may be catalytically activated in the presence of MOF. Both the BET surface area and microporosity of the extrudate were measured to be slightly larger than pristine HKUST-1 powder because of the removal of impurities by methanol immersion. This contributes to the higher gravimetric CO_2 and CH_4 adsorption capacities of the composite compared to the pristine HKUST-1 powder measured at a bulk pressure of up to 10 bar. By using the dual-site Langmuir model, the experimental pure CO_2 and CH_4 isotherms were fitted on both the HKUST-1/PLA extrudate and the HKUST-1 powder. The CO_2 and CH_4 isosteric adsorption heats for the extrudate are similar to those of the pristine HKUST-1 powder. Co-adsorption isotherms and equilibrium selectivities were obtained from the IAST for an equimolar gas mixture. The predicted co-adsorption isotherms demonstrated that CO_2 was more favorably adsorbed than CH_4, but the extrudate's equilibrium selectivities were diminished above 1 bar because more CH_4 was co-adsorbed. At 10 bar and 298 K, the selectivity measured was 5.5, compared to 6.5 at 1 bar. It should be underlined that if textural and gravimetric adsorption capacities were successfully preserved in the extrudate, the reduction in the bulk density of the HKUST-1-PLA composite induces lower volumetric gas adsorption capacities compared to pristine HKUST-1. The presence of PLA was found to have no impact on the stability of pristine HKUST-1 against moisture. This study shows the feasibility of shaping commercial MOF with PLA as a suitable binding agent via extrusion to produce mechanically and thermally resistant adsorbents with good CO_2-CH_4 separation performances.

Supplementary Materials: The following supporting information can be downloaded at: https://www.mdpi.com/article/10.3390/separations10090487/s1, Figure S1: N_2 adsorption isotherm plot for PLA.; Figure S2: Gravimetric adsorption isotherms of CO_2 and CH_4 on PLA.; Figure S3: Gravimetric adsorption-desorption isotherms of CO_2 on HKUST-1 powder, HKUST-1/PLA extrudate and washed HKUST-1 powder.; Figure S4: Gravimetric adsorption isotherms of CO_2 and CH_4 for HKUST-1/PLA extrudate at 273 K, 298 K and 323 K.; Table S1: BET Surface area, pore volume of PLA.

Author Contributions: Conceptualization, D.I.G., P.P. and M.A.B.; data curation, M.T.R.; formal analysis, M.T.R.; funding acquisition, M.A.B. and P.P.; investigation, M.T.R., D.I.G., P.P. and M.A.B.; methodology, M.T.R., D.I.G., P.P. and M.A.B.; project administration, D.I.G., P.P. and M.A.B.; resources, M.A.B. and P.P.; software, D.I.G. and P.P.; supervision, D.I.G., P.P. and M.A.B.; writing—original draft, M.T.R.; writing—review and editing, D.I.G. and P.P. All authors have read and agreed to the published version of the manuscript.

Funding: This research was funded by Yayasan Universiti Teknologi PETRONAS (YUTP)-PRG 2022 grant number 015PBC-014, Yayasan Universiti Teknologi PETRONAS (YUTP)-FRG 2021 grant number 015LC0-36 and IMT Atlantique, providing half a PhD scholarship.

Data Availability Statement: As the data are currently part of an ongoing study, it is not possible to share the raw and processed data required to replicate these findings.

Acknowledgments: The authors thank the Centre of Research in Ionic Liquids, CORIL, Department of Chemical Engineering, Universiti Teknologi PETRONAS, and the Department of Energy Systems and Environment (GEPEA laboratory), IMT Atlantique, for their support in this collaborative work.

Conflicts of Interest: The authors declare no conflict of interest.

References

1. Rafiee, A.; Khalilpour, K.R.; Prest, J.; Skryabin, I. Biogas as an energy vector. *Biomass Bioenergy* **2021**, *144*, 105935. [CrossRef]
2. IEA. Outlook for Biogas and Biomethane: Prospects for Organic Growth. 2020. Available online: https://www.iea.org/reports/outlook-for-biogas-and-biomethane-prospects-for-organic-growth (accessed on 27 July 2023).
3. Kapoor, R.; Ghosh, P.; Kumar, M.; Vijay, V.K. Evaluation of biogas upgrading technologies and future perspectives: A review. *Environ. Sci. Pollut. Res.* **2019**, *26*, 11631–11661. [CrossRef]
4. Adnan, A.I.; Ong, M.Y.; Nomanbhay, S.; Chew, K.W.; Show, P.L. Technologies for Biogas Upgrading to Biomethane: A Review. *Bioengineering* **2019**, *6*, 92. [CrossRef] [PubMed]
5. Aghel, B.; Behaein, S.; Wongwises, S.; Shadloo, M.S. A review of recent progress in biogas upgrading: With emphasis on carbon capture. *Biomass Bioenergy* **2022**, *160*, 106422. [CrossRef]
6. Ahmed, S.F.; Mofijur, M.; Tarannum, K.; Chowdhury, A.T.; Rafa, N.; Nuzhat, S.; Kumar, P.S.; Vo, D.-V.N.; Lichtfouse, E.; Mahlia, T.M.I. Biogas upgrading, economy and utilization: A review. *Environ. Chem. Lett.* **2021**, *19*, 4137–4164. [CrossRef]
7. Hosseini, S.S.; Denayer, J.F. Biogas upgrading by adsorption processes: Mathematical modeling, simulation and optimization approach—A review. *J. Environ. Chem. Eng.* **2022**, *10*, 107483. [CrossRef]
8. Rowsell, J.L.; Yaghi, O.M. Metal–organic frameworks: A new class of porous materials. *Microporous Mesoporous Mater.* **2004**, *73*, 3–14. [CrossRef]
9. Furukawa, H.; Cordova, K.E.; O'Keeffe, M.; Yaghi, O.M. The chemistry and applications of metal-organic frameworks. *Science* **2013**, *341*, 1230444. [CrossRef]
10. Li, B.; Wen, H.-M.; Cui, Y.; Zhou, W.; Qian, G.; Chen, B. Emerging multifunctional metal-organic framework materials. *Adv. Mater.* **2016**, *28*, 8819–8860. [CrossRef]
11. Jiao, L.; Seow, J.Y.R.; Skinner, W.S.; Wang, Z.U.; Jiang, H.-L. Metal–organic frameworks: Structures and functional applications. *Mater. Today* **2019**, *27*, 43–68. [CrossRef]
12. Deyun, M.; Li, Z.; Zhu, J.; Zhou, Y.; Chen, L.; Mai, X.; Liufu, M.; Wu, Y.; Li, Y. Inverse and highly selective separation of CO_2/C_2H_2 on a thulium—Organic framework. *J. Mater. Chem. A* **2020**, *8*, 11933–11937.
13. Letong, L.; Zou, J.; Han, Y.; Liao, Z.; Lu, P.; Nezamzadeh-Ejhieh, A.; Liu, J.; Peng, Y. Recent advances in Al (iii)/In (iii)-based MOFs for the detection of pollutants. *New J. Chem.* **2022**, *46*, 19577–19592.
14. Saha, D.; Bao, Z.; Jia, F.; Deng, S. Adsorption of CO_2, CH_4, N_2O, and N_2 on MOF-5, MOF-177, and zeolite 5A. *Environ. Sci. Technol.* **2010**, *44*, 1820–1826. [CrossRef] [PubMed]
15. Ding, M.; Flaig, R.W.; Jiang, H.-L.; Yaghi, O.M. Carbon capture and conversion using metal-organic frameworks and MOF-based materials. *Chem. Soc. Rev.* **2019**, *48*, 2783–2828. [CrossRef] [PubMed]
16. Abid, H.R.; Hanif, A.; Keshavarz, A.; Shang, J.; Iglauer, S. CO_2, CH_4, and H_2 Adsorption Performance of the Metal–Organic Framework HKUST-1 by Modified Synthesis Strategies. *Energy Fuels* **2023**, *37*, 7260–7267. [CrossRef]
17. Salehi, S.; Anbia, M.; Razavi, F. Improving CO_2/CH_4 and CO_2/N_2 adsorptive selectivity of Cu-BTC and MOF-derived nanoporous carbon by modification with nitrogen-containing groups. *Environ. Prog. Sustain. Energy* **2020**, *39*, 13302. [CrossRef]
18. Teo, H.W.B.; Chakraborty, A.; Kayal, S. Evaluation of CH_4 and CO_2 adsorption on HKUST-1 and MIL-101(Cr) MOFs employing Monte Carlo simulation and comparison with experimental data. *Appl. Therm. Eng.* **2017**, *110*, 891–900. [CrossRef]
19. Asadi, T.; Ehsani, M.R.; Ribeiro, A.M.; Loureiro, J.M.; Rodrigues, A.E. CO_2/CH_4 Separation by Adsorption using Nanoporous Metal organic Framework Copper-Benzene-1, 3, 5-tricarboxylate Tablet. *Chem. Eng. Technol.* **2017**, *36*, 1231–1239. [CrossRef]
20. Ediati, R.; Dewi, S.K.; Hasan, M.R.; Kahardina, M.; Murwani, I.K.; Nadjib, M. Mesoporous HKUST-1 synthesized using solvothermal method. *Rasayan J. Chem.* **2019**, *12*, 1653–1659. [CrossRef]
21. Morales, E.M.C.; Méndez-Rojas, M.A.; Torres-Martínez, L.M.; Garay-Rodríguez, L.F.; López, I.; Uflyand, I.E.; Kharisov, B.I. Ultrafast synthesis of HKUST-1 nanoparticles by solvothermal method: Properties and possible applications. *Polyhedron* **2021**, *210*, 115517. [CrossRef]
22. Nobar, S.N. Cu-BTC synthesis, characterization and preparation for adsorption studies. *Mater. Chem. Phys.* **2018**, *213*, 343–351. [CrossRef]
23. Guo, L.; Du, J.; Li, C.; He, G.; Xiao, Y. Facile synthesis of hierarchical micro-mesoporous HKUST-1 by a mixed-linker defect strategy for enhanced adsorptive removal of benzothiophene from fuel. *Fuel* **2021**, *300*, 120955. [CrossRef]
24. Armstrong, M.; Sirous, P.; Shan, B.; Wang, R.; Zhong, C.; Liu, J.; Mu, B. Prolonged HKUST-1 functionality under extreme hydrothermal conditions by electrospinning polystyrene fibers as a new coating method. *Microporous Mesoporous Mater.* **2018**, *270*, 34–39. [CrossRef]
25. Vehrenberg, J.; Vepsäläinen, M.; Macedo, D.; Rubio-Martinez, M.; Webster, N.A.; Wessling, M. Steady-state electrochemical synthesis of HKUST-1 with polarity reversal. *Microporous Mesoporous Mater.* **2020**, *303*, 110218. [CrossRef]
26. Vepsäläinen, M.; Macedo, D.S.; Gong, H.; Rubio-Martinez, M.; Bayatsarmadi, B.; He, B. Electrosynthesis of HKUST-1 with Flow-Reactor Post-Processing. *Appl. Sci.* **2021**, *11*, 3340. [CrossRef]
27. Liu, P.; Zhao, T.; Cai, K.; Chen, P.; Liu, F.; Tao, D.-J. Rapid mechanochemical construction of HKUST-1 with enhancing water stability by hybrid ligands assembly strategy for efficient adsorption of SF6. *Chem. Eng. J.* **2022**, *437*, 135364. [CrossRef]
28. Tomislav, T.; Batzdorf, L.; Lukin, S.; Žilić, C.; Motillo, C.; Fris, T.; Emmerling, F.; Halasz, I.; Užarević, K. In situ monitoring of the mechanosynthesis of the archetypal metal–organic framework HKUST-1: Effect of liquid additives on the milling reactivity. *Inorg. Chem.* **2017**, *56*, 6599–6608.

29. Ren, J.; Langmi, H.W.; North, B.C.; Mathe, M. Review on processing of metal-organic framework (MOF) materials towards system integration for hydrogen storage. *Int. J. Energy Res.* **2015**, *39*, 607–620. [CrossRef]
30. Ryu, U.; Jee, S.; Rao, P.C.; Shin, J.; Ko, C.; Yoon, M.; Park, K.S.; Choi, K.M. Recent advances in process engineering and upcoming applications of metal–organic frameworks. *Coord. Chem. Rev.* **2021**, *426*, 213544. [CrossRef]
31. Liu, X.-M.; Xie, L.-H.; Wu, Y. Recent advances in the shaping of metal-organic frameworks. *Inorg. Chem. Front.* **2020**, *7*, 2840–2866. [CrossRef]
32. Mallick, A.; Mouchaham, G.; Bhatt, P.M.; Liang, W.; Belmabkhout, Y.; Adil, K.; Jamal, A.; Eddaoudi, M. Advances in Shaping of Metal-Organic Frameworks for CO_2 Capture: Understanding the Effect of Rubbery and Glassy Polymeric Binders. *Ind. Eng. Chem. Res.* **2018**, *57*, 16897–16902. [CrossRef]
33. Ma, Q.; Zhang, T.; Wang, B. Shaping of metal-organic frameworks, a critical step toward industrial applications. *Matter* **2022**, *5*, 1070–1091. [CrossRef]
34. Li, Y.; Wen, G.; Li, J.; Li, Q.; Zhang, H.; Tao, B.; Zhang, J. Synthesis and shaping of metal-organic frameworks: A review. *Chem. Commun.* **2022**, *58*, 11488–11506. [CrossRef] [PubMed]
35. Hong, W.Y.; Perera, S.P.; Burrows, A.D. Manufacturing of metal-organic framework monoliths and their application in CO_2 adsorption. *Microporous Mesoporous Mater.* **2015**, *214*, 149–155. [CrossRef]
36. Gerardo, M.; Pérez-Ramírez, J. Scalable room-temperature conversion of copper (II) hydroxide into HKUST-1 ($Cu_3(btc)_2$). *Adv. Mater.* **2013**, *25*, 1052–1057.
37. Jean, R.; Rouquerol, F.; Llewellyn, P.; Maurin, G.; Sing, K. *Adsorption by Powders and Porous Solids: Principles, Methodology and Applications*; Academic Press: Cambridge, MA, USA, 2013.
38. Khabzina, Y.; Dhainaut, J.; Ahlhelm, M.; Richter, H.-J.; Reinsch, H.; Stock, N.; Farrusseng, D. Synthesis and Shaping Scale-up Study of Functionalized UiO-66 MOF for Ammonia Air Purification Filters. *Ind. Eng. Chem. Res.* **2018**, *57*, 8200–8208. [CrossRef]
39. Myers, A.L.; Prausnitz, J.M. Thermodynamics of mixed-gas adsorption. *AIChE J.* **1965**, *11*, 121–127. [CrossRef]
40. Lee, S.; Lee, J.H.; Kim, J. User-friendly graphical user interface software for ideal adsorbed solution theory calculations. *Korean J. Chem. Eng.* **2018**, *35*, 214–221. [CrossRef]
41. Xiu, D.; Cao, Y.; Shi, X.; Wang, X. Non-isothermal crystallization kinetics, thermal degradation behavior and mechanical properties of poly (lactic acid)/MOF composites prepared by melt-blending methods. *RSC Adv.* **2016**, *6*, 71461–71471.
42. da Silva, F.W.M.; Magalhães, G.M.; de Oliveira Jardim, E.; Silvestre-Albero, J.; Sepúlveda-Escribano, A.; de Azevedo, D.C.S.; de Lucena, S.M.P. CO_2 adsorption on ionic liquid—Modified Cu-BTC: Experimental and simulation study. *Adsorp. Sci. Technol.* **2015**, *33*, 223–242. [CrossRef]
43. Denning, S.; Majid, A.A.; Lucero, J.M.; Crawford, J.M.; Carreon, M.A.; Koh, C.A. Metal-Organic Framework HKUST-1 Promotes Methane Hydrate Formation for Improved Gas Storage Capacity. *ACS Appl. Mater. Interfaces* **2020**, *12*, 53510–53518. [CrossRef] [PubMed]
44. González, S.; Edwin, A.; Olmos, D.; Lorente, M.Á.; Vélaz, I.; González-Benito, J. Preparation and characterization of polymer composite materials based on PLA/TiO_2 for antibacterial packaging. *Polymers* **2018**, *10*, 1365. [CrossRef] [PubMed]
45. Li, Y.; Miao, J.; Sun, X.; Xiao, J.; Li, Y.; Wang, H.; Xia, Q.; Li, Z. Mechanochemical synthesis of Cu-BTC@GO with enhanced water stability and toluene adsorption capacity. *Chem. Eng. J.* **2016**, *298*, 191–197. [CrossRef]
46. Feng, Y.; Jiang, H.; Li, S.; Wang, J.; Jing, X.; Wang, Y.; Chen, M. Metal-organic frameworks HKUST-1 for liquid-phase adsorption of uranium. *Colloids Surfaces A Physicochem. Eng. Asp.* **2013**, *431*, 87–92. [CrossRef]
47. Singbumrung, K.; Motina, K.; Pisitsak, P.; Chitichotpanya, P.; Wongkasemjit, S.; Inprasit, T. Preparation of Cu-BTC/PVA Fibers with Antibacterial Applications. *Fibers Polym.* **2018**, *19*, 1373–1378. [CrossRef]
48. Nivetha, R.; Sajeev, A.; Paul, A.M.; Gothandapani, K.; Gnanasekar, S.; Bhardwaj, P.; Jacob, G.; Sellappan, R.; Raghavan, V.; Chandar, N.K.; et al. Cu based Metal Organic Framework (Cu-MOF) for electrocatalytic hydrogen evolution reaction. *Mater. Res. Express* **2020**, *7*, 114001. [CrossRef]
49. Gwardiak, S.; Szczęśniak, B.; Choma, J.; Jaroniec, M. Benzene adsorption on synthesized and commercial metal–organic frameworks. *J. Porous Mater.* **2019**, *26*, 775–783. [CrossRef]
50. Evans, K.A.; Kennedy, Z.C.; Arey, B.W.; Christ, J.F.; Schaef, H.T.; Nune, S.K.; Erikson, R.L. Chemically Active, Porous 3D-Printed Thermoplastic Composites. *ACS Appl. Mater. Interfaces* **2018**, *10*, 15112–15121. [CrossRef]
51. Mu, X.; Chen, Y.; Lester, E.; Wu, T. Optimized synthesis of nano-scale high quality HKUST-1 under mild conditions and its application in CO_2 capture. *Microporous Mesoporous Mater.* **2018**, *270*, 249–257. [CrossRef]
52. Chen, Y.; Mu, X.; Lester, E.; Wu, T. High efficiency synthesis of HKUST-1 under mild conditions with high BET surface area and CO_2 uptake capacity. *Prog. Nat. Sci.* **2018**, *28*, 584–589. [CrossRef]
53. Shah, B.B.; Kundu, T.; Zhao, D. Mechanical Properties of Shaped Metal-Organic Frameworks. *Top. Curr. Chem.* **2019**, *377*, 25. [CrossRef] [PubMed]
54. Kriesten, M.; Schmitz, J.V.; Siegel, J.; Smith, C.E.; Kaspereit, M.; Hartmann, M. Shaping of Flexible Metal-Organic Frameworks: Combining Macroscopic Stability and Framework Flexibility. *Eur. J. Inorg. Chem.* **2019**, *2019*, 4700–4709. [CrossRef]
55. Zheng, J.; Cui, X.; Yang, Q.; Ren, Q.; Yang, Y.; Xing, H. Shaping of ultrahigh-loading MOF pellet with a strongly anti-tearing binder for gas separation and storage. *Chem. Eng. J.* **2018**, *354*, 1075–1082. [CrossRef]
56. Grande, C.A.; Águeda, V.I.; Spjelkavik, A.; Blom, R. An efficient recipe for formulation of metal-organic Frameworks. *Chem. Eng. Sci.* **2015**, *124*, 154–158. [CrossRef]

57. Cavenati, S.; Grande, C.A.; Rodrigues, A.E. Adsorption Equilibrium of Methane, Carbon Dioxide, and Nitrogen on Zeolite 13X at High Pressures. *J. Chem. Eng. Data* **2004**, *49*, 1095–1101. [CrossRef]
58. Cessford, N.F.; Seaton, N.A.; Düren, T. Evaluation of Ideal Adsorbed Solution Theory as a Tool for the Design of Metal-Organic Framework Materials. *Ind. Eng. Chem. Res.* **2012**, *51*, 4911–4921. [CrossRef]
59. Youn-Sang, B.; Mulfort, K.L.; Frost, H.; Ryan, P.; Punnathanam, S.; Broadbelt, L.J.; Hupp, J.T.; Snurr, R.Q. Separation of CO_2 from CH_4 using mixed-ligand metal-organic frameworks. *Langmuir* **2008**, *24*, 8592–8598.
60. Billemont, P.; Heymans, N.; Normand, P.; De Weireld, G. IAST predictions vs co-adsorption measurements for CO_2 capture and separation on MIL-100 (Fe). *Adsorption* **2017**, *23*, 225–237. [CrossRef]
61. Heymans, N.; Vaesen, S.; De Weireld, G. A complete procedure for acidic gas separation by adsorption on MIL-53 (Al). *Microporous Mesoporous Mater.* **2014**, *154*, 93–99. [CrossRef]
62. Gholipour, F.; Mofarahi, M. Adsorption equilibrium of methane and carbon dioxide on zeolite 13X: Experimental and thermodynamic modeling. *J. Supercrit. Fluids* **2016**, *111*, 47–54. [CrossRef]
63. Garshasbi, V.; Jahangiri, M.; Anbia, M. Equilibrium CO_2 adsorption on zeolite 13X prepared from natural clays. *Appl. Surf. Sci.* **2017**, *393*, 225–233. [CrossRef]
64. Wu, H.; Simmons, J.M.; Srinivas, G.; Zhou, W.; Yildirim, T. Adsorption Sites and Binding Nature of CO_2 in Prototypical Metal-Organic Frameworks: A Combined Neutron Diffraction and First-Principles Study. *J. Phys. Chem. Lett.* **2010**, *1*, 1946–1951. [CrossRef]
65. Supronowicz, B.; Mavrandonakis, A.; Heine, T. Interaction of Small Gases with the Unsaturated Metal Centers of the HKUST-1 Metal Organic Framework. *J. Phys. Chem. C* **2013**, *117*, 14570–14578. [CrossRef]
66. Zhao, Y.; Ge, H.; Miao, Y.; Chen, J.; Cai, W. CO_2 capture ability of Cu-based metal-organic frameworks synergized with amino acid-functionalized layered materials. *Catal. Today* **2020**, *356*, 604–612. [CrossRef]
67. Al-Janabi, N.; Hill, P.; Torrente-Murciano, L.; Garforth, A.; Gorgojo, P.; Siperstein, F.; Fan, X. Mapping the Cu-BTC metal-organic framework (HKUST-1) stability. *Chem. Eng. J.* **2015**, *281*, 669–677. [CrossRef]
68. Terracinaa, A.; Buscarino, G. Water Stability of Metal-Organic Framework HKUST-1. *Gen. Chem.* **2021**, *7*, 210002. [CrossRef]
69. Xue, W.; Zhang, Z.; Huang, H.; Zhong, C.; Mei, D. Theoretical Insights into the Initial Hydrolytic Breakdown of HKUST-1. *J. Phys. Chem. C* **2019**, *124*, 1991–2001. [CrossRef]
70. Michela, T.; Alessi, A.; Luisa, S.; Simonpietro, A.; Marco, C.; Franco, G.; Gianpiero, B. Investigation by Raman Spectroscopy of the Decomposition Process of HKUST-1 upon Exposure to Air. *J. Spectrosc.* **2016**, *2016*, 8074297.
71. Kohlheb, N.; Wluka, M.; Bezama, A.; Thrän, D.; Aurich, A.; Müller, R.A. Environmental-Economic Assessment of the Pressure Swing Adsorption Biogas Upgrading Technology. *BioEnergy Res.* **2021**, *14*, 901–909. [CrossRef]
72. Koonaphapdeelert, S.; Aggarangsi, P.; Moran, J. Biogas Upgrading, in Biomethane. In *Green Energy and Technology*; Springer: Singapore, 2020; pp. 47–98.